

# On the Mott glass in the one-dimensional half-filled charge density waves

Yoshikazu SUZUMURA \* and Masato ISOBE \*\*

*Department of Physics, Nagoya University, Nagoya 464-8602*

(Received )

We study the effect of impurity pinning on a one-dimensional half-filled electron system, which is expressed in terms of a phase Hamiltonian with the charge degree of freedom. Within the classical treatment, the pinned state is examined numerically. The Mott glass, which has been pointed out by Orignac *et al.* [Phys. Rev. Lett **83** (1999)2378], appears in the intermediate region where the impurity potential competes with the commensurate potential. Such a state is verified by calculating the soliton formation energy, the local restoring force around the pinned state and the optical conductivity.

KEYWORDS: Impurity pinning, Mott glass, commensurability pinning, charge fluctuation, soliton formation, optical conductivity

## §1. Introduction

In one-dimensional electron systems, Anderson localization corresponding to the impurity pinning takes place even for weak impurities.<sup>1-3)</sup> The pinning is enhanced for repulsive interactions, as found in the charge density waves<sup>4,5)</sup> where the spatial variation of the phase spreads widely due to randomness.<sup>6)</sup> However, such a pinning becomes complicated for the system with both the commensurate band filling and the repulsive interaction, in which the phase is also pinned by the commensurate potential,<sup>7)</sup> i.e, umklapp scattering. It has been maintained that the Mott insulator with a charge excitation gap occurs for large commensurate potential and the compressive Anderson glass with no excitation gap appears for the weak random impurities.<sup>8,9)</sup> Such a competition has been further investigated by Orignac, Giamarchi and Doussal (OGD),<sup>10)</sup> who applied the variational method to the replicas for the impurity potential. For the case of the impurity potential being much larger than the commensurate potential, one obtains the Anderson glass, in which the optical conductivity exhibits  $\sigma(\omega) \propto \omega^2$  i.e., with no significant effect of the commensurate potential. The opposite case leads to the Mott insulator where the compressibility becomes zero and the gap appears in the optical conductivity. However there exists the intermediate case called the

---

\* E-mail: e43428a@nucc.cc.nagoya-u.ac.jp

\*\* E-mail: isobe@slab.phys.phys.nagoya-u.ac.jp

Mott glass where the compressibility becomes zero but the conductivity shows the gapless behavior similar to that of the Anderson glass.<sup>10,11)</sup> Such a state comes from two kinds of length scales ; one is the localization length and the other is a width of the kink followed by the soliton formation. The vanishing of the compressibility indicates a finite energy to create the soliton of the phase of the charge density wave, i.e., the relevance of the commensurate potential. Thus the energy for the soliton is determined mainly by the local region around the kink. On the other hand, the absence of the gap in the conductivity comes from the property of the impurity pinning with the localization length, which is different from that of the kink. Thus these two kinds of pinning could be compatible and lead to a certain region of coexistence.

Such a coexistence is explored in the present paper by examining the properties of the ground state and the excited state of a system, which lead to the competition between the impurity potential and the commensurate potential. We study numerically a half-filled electron system with repulsive interaction based on the phase Hamiltonian. For the simplicity, we focus on the charge degree of freedom. Based on our preliminary work,<sup>12)</sup> we demonstrate that such a Mott glass state does appear with increasing the commensurate potential as the crossover from the impurity pinning to the commensurability pinning. In §2, formulation is given and the pinned states are examined to determine the competition between the Anderson glass and the Mott glass. In §3, the competition between the Mott glass and the Mott insulator is examined by calculating the local fluctuation around the pinned state, e.g., the restoring force and the optical conductivity. Discussion is given in §4.

## §2. Model and the Pinned State

The formulation for calculating a model numerically is given within the classical treatment. The parameter for the competition between the impurity potential and commensurate potential is derived. The excitation energy for the soliton formation is calculated in the presence of impurity where the appearance of the finite energy is identified with a crossover from the Anderson glass to the Mott glass.

### 2.1 Model

We consider a one-dimensional Hamiltonian with a length  $L$  given by<sup>4)</sup>

$$H = \int_0^L dx \left[ A \left( \frac{d\theta}{dx} \right)^2 - V \sum_{j=1}^{N_{imp}} \cos(\theta + 2k_F x) \delta(x - R_j) - B \cos(2\theta) \right], \quad (1)$$

where  $\theta(x)$  denotes a phase variable of the charge density wave.<sup>13)</sup> The  $V$  term denotes the impurity potential where  $N_{imp}$  is the total number of the impurity and  $R_j$  is the location of the impurity at the  $j$ -th site. Equation (1) without the  $V$  term denotes the Hubbard model with a half-filled band and repulsive interaction,  $U$ ,<sup>14)</sup> in which the quantum fluctuation and the spin degree of freedom are

discarded. Equation (1) describes the classical charge density wave where  $A = v_F/(4\pi)$ ,  $B \sim U/a$  with Fermi velocity,  $v_F$ , and the lattice constant,  $a$ ,<sup>13)</sup> The  $A$  term leads to the uniform  $\theta(x)$  while the  $V$  term and the  $B$  term lead to spatially varying  $\theta(x)$ . We consider the  $A$  term is much larger than the  $V$  term and the  $B$  term, i.e.,  $AN_{imp}/L \gg V$  and  $A(N_{imp}/L)^2 \gg B$ . In such a case, the length corresponding to the impurity concentration is much smaller compared with the characteristic length determined by  $V$  and  $B$  terms. By taking the average spacing of the impurity,  $L/N_{imp}$ , as a new lattice constant, eq. (2) is rewritten as the following discretized model.<sup>15)</sup>

$$H = \sum_{j=1}^{N_{imp}} \left[ An_i(\theta_{j+1} - \theta_j)^2 - V \cos(\theta_j - \zeta_j) - \frac{B}{n_i} \cos(2\theta_j) \right] , \quad (2)$$

where  $n_i = N_{imp}/L$  and  $\zeta_j (= -2k_F R_j)$  is a random variable with a Fermi momentum  $k_F$ . The characteristic length  $l_0$ , which denotes the pinning by the impurity potential, is determined by the following variational method. Considering eq.(2) with  $B = 0$ , one obtains the energy gain of the second term given by  $-V/\sqrt{n_i l_0}$  per lattice site, but the increase of the first term given by  $\simeq A/n_i l_0^2$ . Minimizing the total energy consisting of these two quantities, one obtains  $l_0$  as<sup>6)</sup>

$$n_i l_0 = \left( \frac{K_0}{\pi \epsilon} \right)^{\frac{2}{3}} , \quad (3)$$

where  $K_0 = \pi^2/3$  and

$$\epsilon = \frac{V}{4\pi An_i} . \quad (4)$$

The present paper treats the case of small  $\epsilon (\ll 1)$  corresponding to the weak impurity pinning. On the other hand, eq. (2) with  $V = 0$  gives the excitation followed by the soliton formation with an energy,  $4\sqrt{2}(AB)^{1/2}$ , and a characteristic length  $d$ ,

$$d \equiv \left( \frac{2A}{B} \right)^{1/2} . \quad (5)$$

Since  $l_0$  is the pinning length for the  $V$  term and  $d$  is the width of the soliton for the  $B$  term, the competition between these two terms is characterized by the quantity<sup>7)</sup>

$$\bar{l}_0 = \frac{l_0}{d(2K_0)^{\frac{1}{2}}} . \quad (6)$$

It is expected that the crossover from the impurity pinning to the commensurability pinning occurs for  $\bar{l}_0 \sim o(1)$ .

For the convenience of the numerical calculation, eq. (2) is rewritten as

$$H = An_i \sum_{j=1}^{N_{imp}} \left[ (\theta_{j+1} - \theta_j)^2 - 4\pi\epsilon \cos(\theta_j - \zeta_j) - \beta \cos(2\theta_j) \right] , \quad (7)$$

where

$$\beta = \frac{B}{An_i^2} = 4 \frac{(\pi\epsilon)^{\frac{4}{3}}}{K_0^{\frac{1}{3}}} \bar{l}_0^{-2} . \quad (8)$$

Equation (7) shows that the energy is measured in the unit of  $An_i$  and the lattice constant is taken as  $1/n_i$ . By minimizing eq. (7) with respect to  $\theta_j$ , we obtain the equation for  $\theta_j$  as

$$(2\theta_j - \theta_{j+1} - \theta_{j-1}) + 4\pi\epsilon \sin(\theta_j - \zeta_j) + 2\beta \sin(2\theta_j) = 0 \quad , \quad (9)$$

where  $j = 1, \dots, N$ . A periodic boundary condition is taken where  $\theta_0 = \theta_{N_{imp}}$  and  $\theta_{N_{imp}+1} = \theta_1$ .

The following calculation is performed by taking two kinds of parameters,  $\epsilon$  and  $\bar{l}_0$  which correspond to the variation of  $V$  and  $B$  respectively.

### 2.2 spatial variation of $\theta_j$

We calculate eq. (9) iteratively with several choices of initial values and stop the calculation when the absolute value of the l.h.s. becomes less than  $10^{-7}$ . The strength of the impurity pinning is chosen as  $\epsilon = 0.01$ , which denotes the weak pinning and leads to the pinning length,  $n_i l_0 \sim 22$ . In this case, considering the periodic boundary condition, one expects that there are about ten regions of  $\theta_j$  exhibiting the rapid variation of the order of  $\pi$  for a system with  $N_{imp} = 400$ .

In Fig. 1, we show the numerical results for  $N_{imp} = 400$ ,  $\epsilon = 0.01$ ,  $\bar{l}_0 = 0, 0.5$  and  $1.5$  respectively. There are many solutions corresponding to the metastable states, which have the energy close to the ground state. Figure 1 may be regarded as the ground state since the corresponding energy is the lowest one within the present calculation. The variation of  $\theta_j$  becomes small with increasing  $\bar{l}_0$  i.e., the commensurability energy. Such a state is the solution for the uniform sector since the spatial variation becomes constant (e.g.  $\theta_j = 0$ ) in the limit of large  $\bar{l}_0$ .

Figure 2 shows the spatial variation of  $\theta_j$  for the excited state in which the soliton exists. For  $\bar{l}_0 \gtrsim 1.4$ , one of the the kinks is found at  $x_j \simeq 170$  although the initial value of the kink is taken at  $x_j = 200$ . This indicates that the kink is determined in order to gain the energy from the impurity potential even for the large  $\bar{l}_0$ . The kink begins to move from  $x_j \simeq 170$  to  $x_j \simeq 140$  with decreasing  $\bar{l}_0$  while the other kink also moves at lower  $\bar{l}_0$  to gain the energy from the impurity potential. However the location is fixed for the case of  $\bar{l}_0 \lesssim 0.6$  indicating a crossover from the commensurability pinning to the impurity pinning. Such a state is regarded as the solution from the soliton sector since the spatial variation reduces to the solution of the soliton-antisoliton in the limit of large  $\bar{l}_0$ .

### 2.3 excitation energy

There are two kinds of excitations from the ground state. One of them is the excitation within the uniform sector, which is gapless one due to the continuous distribution of the energy. The other is the excitation followed by the soliton formation where the lowest one is a state with the soliton-antisoliton. The energy difference between these two states,  $\delta E_{exc}$ , is calculated by

$$\delta E_{exc} = \delta E_{sol} - \delta E_{ground} \quad . \quad (10)$$

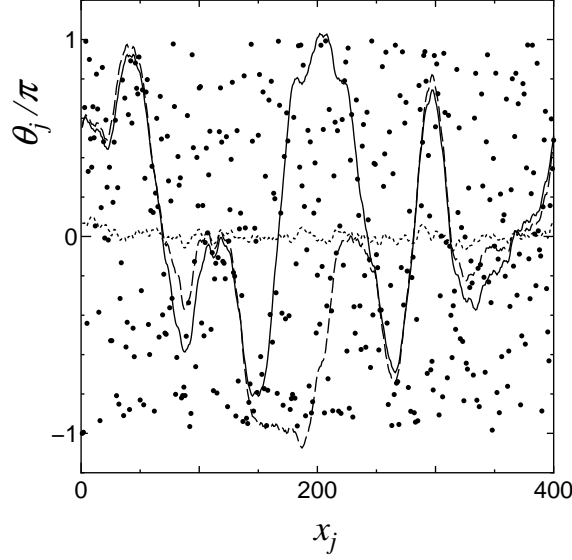


Fig. 1. Spatial variation of  $\theta_j$  for  $N_{imp} = 400$ ,  $\epsilon = 0.01$  with fixed  $\bar{l}_0 = 0$  (solid line), 0.5 (dashed line) and 1.5 (dotted line). The unit of  $x_j (= 1, \dots, N_{imp})$  is given by  $1/n_i$ .

Quantities  $\delta E_{sol}$  and  $\delta E_{ground}$ , which denote the deviation of the the energy from that of the state with  $\theta_j = 0$ , are calculated by substituting  $\theta_j$  of the respective sector into the following equation:

$$\begin{aligned} \delta E &\equiv \left( \frac{E}{L} + B \right) / (3AK_0/l_0^2) \\ &= \frac{1}{\pi^2 N_{imp}} \left( \frac{\pi}{3\epsilon} \right)^{\frac{4}{3}} \sum_{j=1}^{N_{imp}} \left[ (\theta_{j+1} - \theta_j)^2 - 4\pi\epsilon \cos(\theta_j - \epsilon_j) - \beta \cos(2\theta_j) \right] + \frac{4}{3} \bar{l}_0^{-2} \quad , \quad (11) \end{aligned}$$

where  $E$  denotes an expectation value of  $H$  given by eq. (1).

It should be noted that there is a critical value  $\bar{l}_S (\simeq 0.6)$  as shown by the arrow in Fig. 3 where  $\delta E_{exc} (> 0)$  is very small and almost constant for  $\bar{l}_0 < \bar{l}_S$ . Although the spatial variation of the soliton sector is apparently retained even for small  $\bar{l}_0$ , the effect of the commensurability energy is negligibly small and then such a spatial variation can be regarded as one of the metastable states in the absence of the commensurability energy. For  $\bar{l}_0 \gtrsim \bar{l}_S$ , one obtains  $\delta E_{exc} \sim 0.25\bar{l}_0 - 0.8$ , which indicates that the formation energy of soliton-antisoliton is finite but is reduced by a finite energy due to the energy gain by the impurity potential.

### §3. Fluctuation around the Pinned State

In order to find the crossover from the Mott glass to the Mott insulator, the degree of the local charge fluctuation around the ground state is examined by calculating the response to the external field, which gives rise to the optical conductivity.

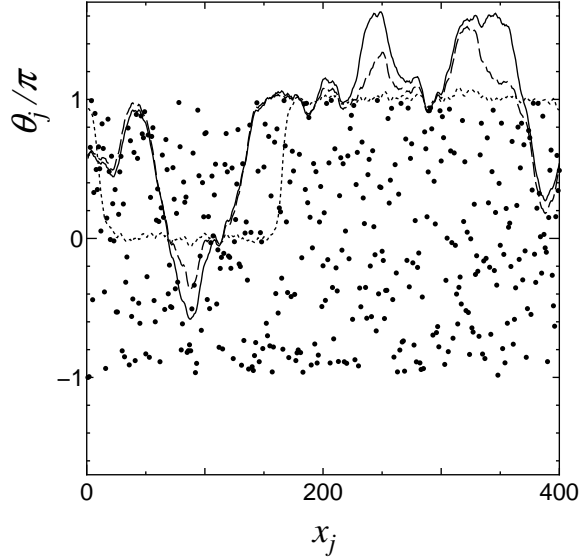


Fig. 2. Spatial variation of  $\theta_j$  for  $N_{imp} = 400$ ,  $\epsilon = 0.01$  for the excited state followed by a formation of a soliton-antisoliton where  $\bar{l}_0 = 0$  (solid line), 0.5 (dashed line) and 1.5 (dotted line).

### 3.1 local pinning frequency $\omega_j$

We examine the restoring force for  $\theta_j$  at the  $j$ -th site when the small deviation of  $\theta_j$  occurs from the equilibrium value. The magnitude of the force depends on the location of the lattice site since the pinning comes from not only the commensurate potential but also the impurity potential. Such a quantity is estimated from the increase of the energy by adding the external electric field  $E'$  which gives an additional term,  $-E\theta$ , to the r.h.s. of eq.(1) where  $E = eE'/\pi$  with  $e$  being the electric charge.<sup>16)</sup> In this case, the lattice model is rewritten as

$$H = An_i \sum_{j=1}^{N_{imp}} \left[ (\theta_{j+1} - \theta_j)^2 - 4\pi\epsilon \cos(\theta_j - \zeta_j) - \beta \cos(2\theta_j) - \gamma \bar{E} \theta_j \right] , \quad (12)$$

where  $\bar{E} = \bar{l}_0^2 / (3AK_0)$  and

$$\gamma \equiv \frac{3(\pi\epsilon)^{\frac{4}{3}}}{K_0^{\frac{1}{3}}} . \quad (13)$$

The resultant equation for  $\theta_j$  is given by

$$(2\theta_j - \theta_{j+1} - \theta_{j-1}) + \alpha \sin(\theta_j - \zeta_j) + 2\beta \sin(2\theta_j) - \gamma \bar{E} = 0 . \quad (14)$$

By using  $\theta_j(E)$  of the solution of eq. (14), we calculate

$$1/\omega_j^2 = \lim_{\bar{E} \rightarrow 0} (\theta_j(E) - \theta_j(0)) / \gamma \bar{E} . \quad (15)$$

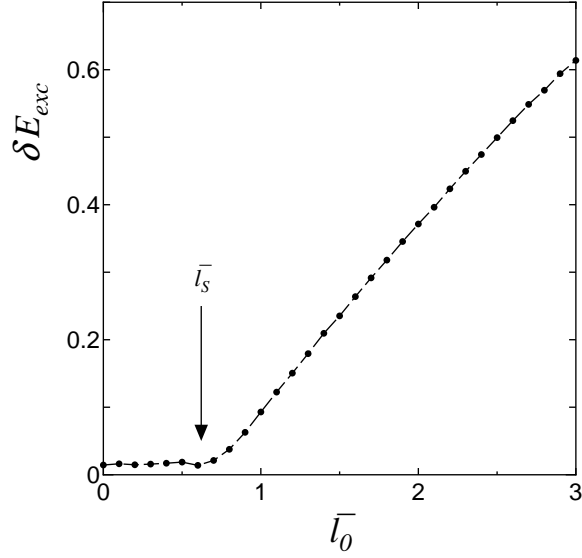


Fig. 3. Excited energy  $\delta E_{exc}$  as a function of  $\bar{l}_0$  for  $N_{imp} = 400$  and  $\epsilon = 0.01$ , which is averaged over 400 samples. The arrow  $\bar{l}_s$  denotes a critical value above which the soliton formation is followed by a finite energy.

The quantity  $\omega_j$  is the local pinning frequency since the increase of the energy in the presence of the small external field can be expressed as  $\omega_j^2(\theta_j(E) - \theta_j(0))^2/2$ , which is calculated by expanding eq. (12) in terms of  $\theta_j(E) - \theta(0)$ .

In Fig. 4,  $\bar{l}_0$  dependence of  $\langle \omega_j \rangle$  is shown for  $N_{imp} = 4000$  and  $\epsilon = 0.01$  where  $\langle \rangle$  denotes the spatial average and the closed square is the result averaged over 20 samples. The calculation of  $\omega_j$  has been performed by choosing  $\bar{E} = 0.001$ , which is small enough to calculate eq. (15). For  $\bar{l}_0 \lesssim 0.4$ , the quantity  $\langle \omega_j \rangle$  is constant indicating no visible effect of the commensurability pinning. The commensurability pinning dominates for  $\bar{l}_0 \gtrsim 0.6$ , in which  $\omega_j \propto \bar{l}_0$ . It seems that a crossover from the impurity pinning to the commensurability pinning occurs in the interval region of  $0.4 \lesssim \bar{l}_0 \lesssim 0.6$ .

### 3.2 root mean square of $\omega_j$

The property of the spatial variation of  $\omega_j$  is examined by calculating the root mean square of  $\omega_j$ . The normalized root mean square of  $\omega_j$  is given by

$$z = \frac{1}{\langle \omega_j \rangle} \sqrt{\langle (\omega_j - \langle \omega_j \rangle)^2 \rangle}. \quad (16)$$

The larger  $z$  indicates the broader distribution of the pinning force. It is expected that  $z$  of the impurity pinning is much larger than that of the commensurability pinning. The fluctuation of  $z$  is large for the choice of the present sample with  $N_{imp}$  where  $z_s$  is used to distinguish the respective

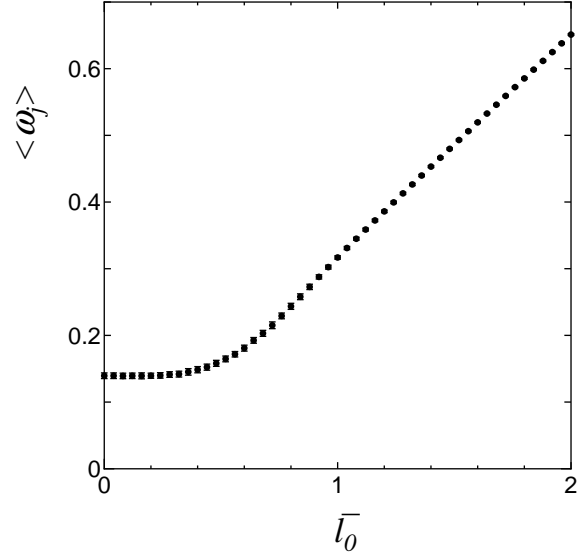


Fig. 4.  $\bar{t}_0$  dependence of  $\langle \omega_j \rangle$  for  $N_{imp} = 4000$  and  $\epsilon = 0.01$ , which is averaged over 20 samples. The limiting behavior is evaluated by taking  $\bar{E} = 0.001$ . The error bar becomes negligibly small in the visible scale with increasing  $\bar{t}_0$ .

sample. Thus, we further examine the root mean square of  $z_s$  given by

$$\sqrt{\langle (z_s - \langle z_s \rangle)^2 \rangle} . \quad (17)$$

Figure 5 (dashed line and closed circle) shows the normalized root mean square of  $\langle \omega_j \rangle$ , i.e.  $\langle z_s \rangle_s$  for  $N_{imp} = 400$ ,  $\epsilon = 0.01$  and  $\bar{E} = 0.001$  where 400 samples are used for  $s$ . For  $\bar{t}_0 \lesssim 0.6$ ,  $\langle z_s \rangle_s$  is almost constant while it decreases for  $\bar{t}_0 \gtrsim 0.6$  due to the increase of the commensurability pinning. The result for the soliton sector is shown by the open circle where it remains finite even for large  $\bar{t}_0$ . This is understood as follows. When the impurity is absent, the location of the kink is easy to move under the external field resulting in the extremely small  $\omega_j$ . However the presence of the impurity pinning prevents such a movement leading to finite  $\omega_j$ , which gives the variation similar to the impurity pinning. The deviation from that of the uniform sector is found for  $\bar{t}_0 \gtrsim 0.7$ , which is slightly larger than  $\bar{t}_S$ . This indicates a possibility that the fluctuation around the pinned state even for  $\bar{t}_0 \gtrsim \bar{t}_S$  still resembles that of  $\bar{t}_0 = 0$ . The inset shows the root mean square of such  $z_s$  which gives a critical value  $\bar{t}_0 \simeq 1.0$ , above which the spatial fluctuation of  $\omega_j$  decreases rapidly indicating a crossover into the Mott insulating state.



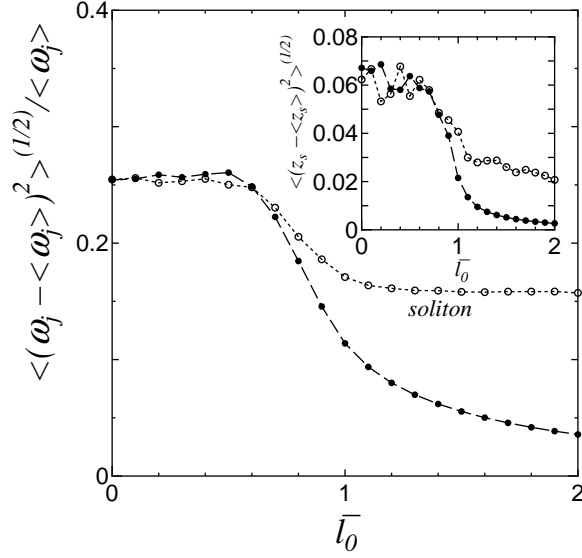


Fig. 5.  $\bar{l}_0$  dependence of the normalized root mean square of  $\omega_j$  for  $N_{imp} = 400$ ,  $\epsilon = 0.01$  and  $\bar{E} = 0.001$  which is averaged over 400 samples. The closed circle and solid line (open circle and dotted line) denote the results for the ground state (the excited state with soliton). The inset denotes the corresponding root mean square of  $z_s$  given by  $\sqrt{\langle (z_s - \langle z_s \rangle)^2 \rangle}$ .

This tendency can be also seen from the distribution of  $\omega_j$ , which is defined by

$$P(\omega) = \frac{1}{N_{imp}} \sum_{j=1}^{N_{imp}} \delta(\omega - \omega_j) . \quad (18)$$

In Fig. 6,  $\omega (= \omega_j)$  dependence of  $P$  is shown for  $N_{imp} = 4000$ ,  $\epsilon = 0.01$  and  $\bar{E} = 0.001$  where  $\bar{l}_0 = 0$  (closed circle), 0.5 (open circle), 0.8 (closed triangle) and 1.5 (closed diamond). The average over 20 samples are used for the numerical accuracy of small  $\omega$ . The quantity  $P$  with  $\bar{l}_0 = 0$  is almost the same as  $P$  with  $\bar{l}_0 = 0.5$  and still resembles  $P$  with  $\bar{l}_0 = 0.8$  while it is much different from  $P$  with  $\bar{l}_0 = 1.5$ . This indicates that the distribution changes the property for  $\bar{l}_0 > \bar{l}_G$ , where  $\bar{l}_G$  is larger than at least 0.8.

### 3.3 optical conductivity

Based on Figs. 3, 4, 5 and 6, it is reasonable to admit that the intermediate region with  $\bar{l}_S < \bar{l}_0 < \bar{l}_G$  may correspond to that of the Mott glass. However the estimation for  $\bar{l}_G$  is rather complicated compared with  $\bar{l}_S$ . Then we examine the optical conductivity since the Mott glass is maintained to exhibit the optical conductivity given by  $\sigma(\omega) \propto \omega^2$ .<sup>10)</sup> We calculate the conductivity within the

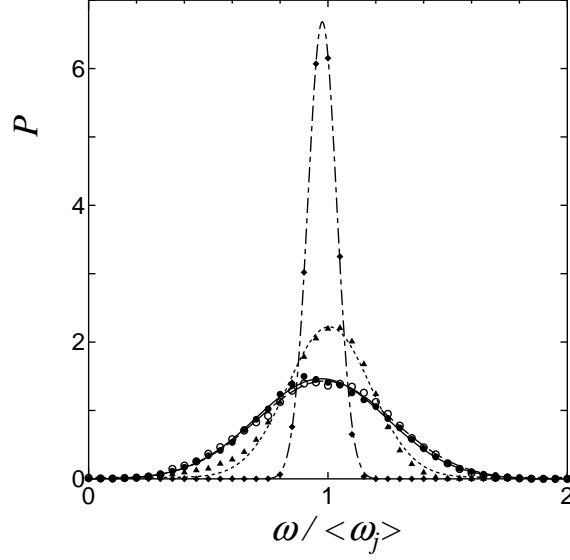


Fig. 6. Normalized distribution of  $\omega_j$ ,  $P(\omega / \langle \omega_j \rangle)$ , for  $N_{imp} = 4000$ ,  $\epsilon = 0.01$  and  $\bar{E} = 0.001$  where  $\bar{l}_0 = 0$  (closed circle), 0.5 (open circle), 0.8 (closed triangle) and 1.5 (closed diamond). The results are obtained by averaging over 20 samples.

classical treatment, by noting the fact that the electric dipole moment at the  $j$ -th site is given by  $(2k_F/\pi)ey_j = (e/\pi)\theta_j$  with  $y_j$  being the displacement.<sup>16)</sup> In the presence of the electric field  $E_0e^{i\omega t}$ , the equation of motion for the charge density wave is given by

$$m^* \frac{d^2 y_j}{dt^2} = -\frac{m^*}{\tau} \frac{dy_j}{dt} + eE_0 e^{i\omega t} - m^* \omega_j^2 y_j, \quad (19)$$

where  $m^*$  is the effective mass and the life time,  $\tau$ , is introduced for the convergence of the numerical calculation. The quantity  $\omega_j$ , which corresponds to the restoring force,  $m^* \omega_j^2 y_j$  is calculated from eq. (15). The quantity  $y_j$  is calculated as

$$y_j = \frac{eE_0/(i\omega m^*)}{\frac{1}{\tau} + i\omega \left(1 - \frac{\omega_j^2}{\omega^2}\right)}, \quad (20)$$

which leads to the local conductivity at the  $j$ -th site

$$\sigma_j(\omega) = \frac{2k_F e^2 \tau}{m^* \pi} \frac{1}{1 + i\omega\tau \left(1 - \frac{\omega_j^2}{\omega^2}\right)}. \quad (21)$$

Thus one obtains the real part of the total conductivity as

$$\sigma(\omega) = \frac{2\tau}{\pi N_{imp}} \sum_{j=1}^{N_{imp}} \frac{1}{1 + (\omega\tau)^2 \left(1 - \frac{\omega_j^2}{\omega^2}\right)^2}, \quad (22)$$

where the conductivity is normalized such that the summation of  $\sigma(\omega)$  with respect to  $\omega$  becomes equal to unity. In Fig. 7, optical conductivity is shown for  $N_{imp} = 4000$ ,  $\epsilon = 0.01$  and  $\tau = 20$  where respective results are for  $\bar{l}_0 = 0$  (closed circle), 0.5 (open circle), 0.8 (closed ) and 1.5 (closed diamond). The conductivity for  $\bar{l}_0 = 0$  denotes the conventional impurity pinning of the charge

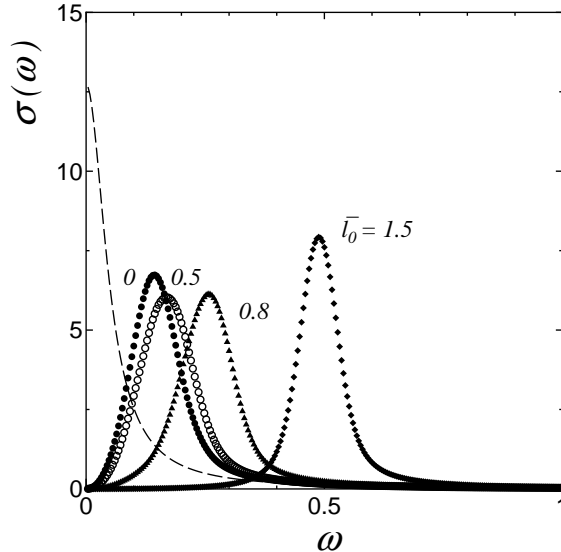


Fig. 7. Normalized optical conductivity for  $N_{imp} = 400$ ,  $\epsilon = 0.01$  and  $\tau = 20$ , which are averaged over 100 samples. Respective results are for  $\bar{l}_0 = 0$  (closed circle), 0.5 (open circle), 0.8 (closed ) and 1.5 (closed diamond). The dashed curve corresponds to the conductivity of the Drude's formula (i.e.,  $\omega_j \rightarrow 0$ ).

density wave where the frequency of  $\omega$  corresponding to the peak is essentially the same as  $\langle \omega_j \rangle$ , i.e., the average of  $\omega_j$  shown in Fig. 4. Such a frequency increases with increasing  $\bar{l}_0$ , which is consistent with the result of Fig. 4. The width of  $\omega$  is determined by the root mean square of  $\omega_j$ , (Fig. 5). The width for small  $\bar{l}_0$ , which is determined by the distribution of the pinning force, decreases for large  $\bar{l}_0$  due to the increase of the commensurability pinning. It is found that the peak of  $\omega$  is slightly reduced in region of the Mott glass ( $\bar{l}_S < \bar{l}_0 < \bar{l}_G$ ), since the width of  $\sigma(\omega)$  in the Mott glass becomes large due to the competition between the impurity pinning and the commensurability pinning. For comparison, the conductivity of the Drude's formula is shown by the dashed curve where the width is chosen as  $\tau = 20$ . The conductivity for  $\bar{l}_0 = 0, 0.5$  and 0.8 exhibits  $\sigma(\omega) \propto \omega^2$  for small  $\omega$  within the numerical accuracy of the present calculation indicating the property of the Anderson glass. In order to examine such a region, we calculate a coefficient,  $A$ , of  $\sigma(\omega)$  which is given in the limit of small  $\omega$  by

$$\sigma(\omega) \simeq A\omega^2 . \quad (23)$$

In Fig. 8, the quantity  $A$  is shown by taking  $\omega \rightarrow 0.01$ , where the dashed line denotes the guide for the eye. The inset depicts the procedure to calculate  $A$  by an extrapolation of  $A(\tau)$  for  $1/\tau = 1, 0.1$  and  $0.05$  since eq. (23) depends on  $\tau$ . With increasing  $\bar{l}_0$ , the quantity  $A$  stays almost constant for small  $\bar{l}_0$  while it decreases rapidly for  $\bar{l}_0 \simeq 1.0$ . However, the data for  $\bar{l}_0 > 1.0$  is beyond the present calculation, which is based on the model of the classical charge density wave, and eq. (22) showing the gradual decrease of  $A$  even in the Mott insulating phase. Thus we conclude  $\bar{l}_G \simeq 1.0$ , which is shown by the arrow in the main figure.

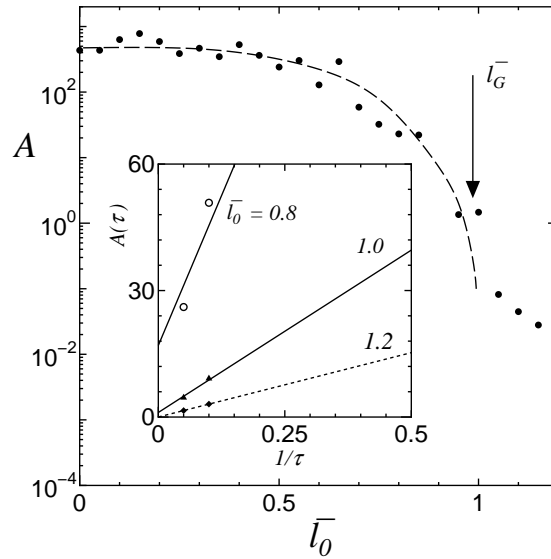


Fig. 8.  $\bar{l}_0$  dependence of  $A$ , which denotes  $\sigma(\omega) \simeq A\omega^2$  in the limit of small  $\omega$ . In the inset,  $A$  is obtained from the value of the vertical axis where the extrapolation for  $1/\tau$  is shown for  $\bar{l}_0 = 0.8, 1.0$  and  $1.2$ . The steep decrease of  $A$  leads to  $\bar{l}_G \simeq 1.0$  as shown by the arrow.

#### §4. Discussion

We have examined the competition between the impurity pinning and the commensurability pinning of the charge density wave, which leads to three kinds of phases as a crossover. It is found that the Mott glass state exists in the intermediate region of  $\bar{l}_S < \bar{l}_0 < \bar{l}_G$  with  $\bar{l}_S \simeq 0.6$  and  $\bar{l}_G \simeq 1.0$  while there are the region of the Anderson glass for  $\bar{l}_0 < \bar{l}_S$  and that of the Mott insulator for  $\bar{l}_G < \bar{l}_0$ .

The intermediate region corresponding to the Mott glass seems to be consistent with that of OGD,<sup>10)</sup> who obtained  $0.98 < d/\bar{l}_0 < 1.58$  in their notations. The Mott glass undergoes the crossover to the Anderson glass (or Mott insulator) with decreasing (or increasing)  $\bar{l}_0$  due to the effect of the impurity, which has the wide distribution of the pinning force (i.e. restoring force).

Then there is a tiny domain of the soliton formation in the state of the Mott glass. Even in the presence of such a state, the optical conductivity similar to the Anderson glass could be expected due to the contribution from the slowly varying region<sup>17)</sup> since the conductivity originates in the distribution of the restoring force in the uniform sector. The conductivity with low frequency resembles that of the Anderson glass, which denotes no gap in the conductivity, i.e.,  $\sigma(\omega) \propto \omega^2$  for small  $\omega$ . Note that it is beyond the present calculation to examine if the conductivity exhibits a property  $\sigma(\omega) \propto \omega^2 \ln^2(\omega\tau)$ .<sup>1,2)</sup> The existence of the gap for the formation of the phase soliton, which leads to the variation of the electron number, is equivalent to the absence of compressibility since a finite energy is needed to add or remove an electron. However the case of doping of electron or hole, which corresponds to the ground state with the soliton formation, leads to the absence of the Mott insulator and the optical conductivity with no gap as expected from the soliton sector of Fig. 5.

Here we comment on the present mode of the charge density wave, which is relevant to the electron system. The latter case includes two additional factors, i.e, the quantum fluctuation and the spin fluctuation. These factors have at least the effect of reducing the magnitude of  $V$  and  $B$  in eq. (2), which could be taken into account by adjusting parameters. However the novel effect can be expect when the depinning begins. This problem will be discussed in a separate paper.

- 
- 1) V.L. Berezinskii: Zh. Eksp. Teor. Fiz. **65**(1973)1251 [Sov. Phys.-JETP **38** (1974) 620].
  - 2) M.V. Feigelman and Vinokur: Solid State Commun. **45** (1983) 603
  - 3) E. Abraham, P.W. Anderson, D.C. Licciardello and T.V. Ramakrishnan: Phys. Rev. Lett **42** (1979) 673.
  - 4) Y. Suzumura and H. Fukuyama: J. Phys. Soc. Jpn. **53** (1984) 3918.
  - 5) T. Giamarchi and H.J. Schulz: Phys. Rev. B **37** (1988) 325.
  - 6) H. Fukuyama and P.A. Lee: Phys. Rev. B **17** (1978) 535.
  - 7) H. Fukuyama: J. Phys. Soc. Jpn. **45** (1978) 1474.
  - 8) S. Fujimoto and N. Kawakami: Phys. Rev. B **54** (1996) R11018.
  - 9) M. Mori and H. Fukuyama: J. Phys. Soc. Jpn. **65** (1996) 3604.
  - 10) E. Orignac, T. Giamarchi and P. Le Doussal: Phys. Rev. Lett **83** (1999) 2378.
  - 11) S. Fujimoto: J. Phys. Soc. Jpn. **69** (2000) 2597.
  - 12) Y. Suzumura and M. Isobe: read at Meeting of Physical Society of Japan, Sendai, March 28-31, 2003.
  - 13) Y. Suzumura: Prog. Theor. Phys. **61** (1979) 1.
  - 14) J. Sólyom: Adv. Phys. **28** (1979) 201.
  - 15) Y. Suzumura and T. Saso: J. Phys. Soc. Jpn. **55** (1986) 4359.
  - 16) H. Fukuyama: J. Phys. Soc. Jpn. **41** (1976) 513.
  - 17) T. Giamarchi, P. Le Doussal and E. Orignac: Phys. Rev. B **64** (2001) 245119.